

Checking the dark matter origin of 3.53 keV line with the Milky Way center

A. Boyarsky¹, J. Franse^{1,2}, D. Iakubovskiy³, and O. Ruchayskiy⁴

¹Instituut-Lorentz for Theoretical Physics, Universiteit Leiden, Niels Bohrweg 2, Leiden, The Netherlands

²Leiden Observatory, Leiden University, Niels Bohrweg 2, Leiden, The Netherlands

³Bogolyubov Institute of Theoretical Physics, Metrologichna Str. 14-b, 03680, Kyiv, Ukraine

⁴Ecole Polytechnique Fédérale de Lausanne, FSB/ITP/LPPC, BSP, CH-1015, Lausanne, Switzerland

(■Dated: August 12, 2014)

We detect a line at 3.539 ± 0.011 keV in the deep exposure dataset of the Galactic Center region, observed with the XMM-Newton. Although it is hard to completely exclude an astrophysical origin of this line in the Galactic Center data alone, the dark matter interpretation of the signal observed in the Perseus galaxy cluster and Andromeda galaxy [1] and in the stacked spectra of galaxy clusters [2] is fully consistent with these data. Moreover, the Galactic Center data support this interpretation as the line is observed at the same energy and has a flux consistent with the expectations about the Galactic dark matter distribution for a class of the Milky Way mass models.

Recently, two independent groups [1, 2] had reported a detection of an unidentified X-ray line at energy 3.53 keV in the long-exposure X-ray observations of a number of dark matter-dominated objects. The work [2] has observed this line in a stacked XMM spectrum of 73 galaxy clusters spanning a redshift range 0.01–0.35 and separately in subsamples of nearby and remote clusters. Ref. [1] have found this line in the outskirts of the Perseus cluster and in the central 14' of the Andromeda galaxy. The global significance of the detection of the same line in the datasets of Ref. [1] is 4.3σ (taking into account the trial factors); the signal in [2] has significance above 4σ on completely independent data.

The position of the line is correctly redshifted between galaxy clusters [2] and between the Perseus cluster and Andromeda galaxy [1]. In a very long exposure blank sky observation (15.7 Msec of cleaned data) the feature is absent [1]. This makes an instrumental origin of this feature (e.g. an unmodulated wiggle in the effective area) unlikely.

To identify this spectral feature with an atomic line in galaxy clusters, one should assume a strongly super-solar abundance of potassium or some anomalous argon transition [2]. Moreover, according to the results of [1], this should be true not only in the center of the Perseus cluster, considered in [2], but also (i) in its outer parts up to at least 1/2 of its virial radius and (ii) in the Andromeda galaxy.

This result triggered significant interest as it seems consistent with a long-sought for signal from decaying dark matter. Many particle physics models, predicting such properties of dark matter particles, have been put forward. This includes the sterile neutrino, axion, axino and many others [3–57]. If the interaction of dark matter particles is weak enough (e.g. much weaker than that of the Standard Model neutrino), they need not be stable as their lifetime can exceed the age of the Universe. Nevertheless humongous amounts of dark matter particles make the signal even from such rare decays strong enough to be detectable.

The omni-presence of dark matter in galaxies and galaxy clusters opens the way to check the decaying dark matter hypothesis [58]. The decaying dark matter signal is proportional to the *column density* $S_{\text{DM}} = \int \rho_{\text{DM}} d\ell$ – integral along the line of sight of the DM density distribution (unlike the case of annihilating dark matter, where the signal is proportional to $\int \rho_{\text{DM}}^2 d\ell$). As long as the angular size of an object is larger than the field-of-view, the distance to the object drops out which means that distant objects can give a comparable signal to the nearby ones [59, 60]. It also does not decrease with the distance from the centres of objects as fast as e.g. in the case of annihilating DM where the expected signal is concentrated towards the centers of DM-dominated objects. This in principle allows one to check the dark matter origin of a signal by comparison between objects and/or by studying angular dependence of the signal within one object, rather than trying to exclude all possible astrophysical explanations for each target [61–64].

However, in reality, of course, after years of systematic searches for this signal [61, 65–90], any candidate line can be detected only at the edge of possible sensitivity of the method. Therefore, to cross-check the signal one needs comparably long exposure data. Moreover, even the uncertainty at the level of factor of few in the expected signal, which is very hard to avoid, results in the necessity to have significantly more statistics than in the initial data set, where a candidate signal was found.

So far DM interpretation of the signal of [2] and [1] is consistent with the data: it has correct scaling between Perseus cluster, Andromeda galaxy and the upper bound from non-detection in the blank sky data [1], between different subsamples of clusters [2]. Mass and lifetime of the dark matter particle, implied by DM interpretation of results of [1], is consistent with the results of [2]. The signal also has a radial surface brightness profiles in the Perseus cluster and Andromeda galaxy [1] that are consistent with dark matter distribution.

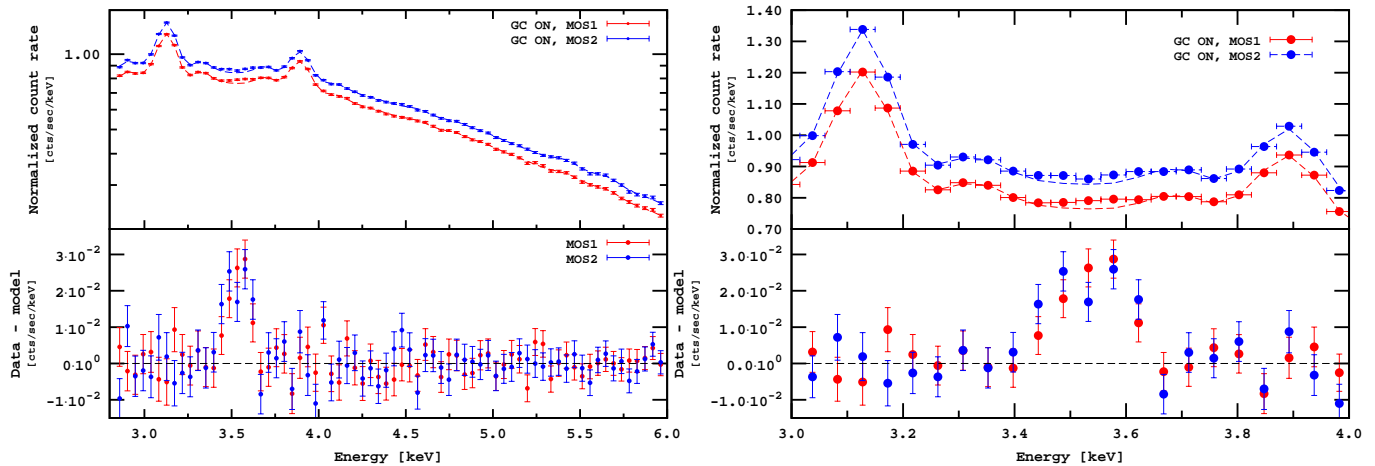


FIG. 1: *Left*: Folded count rate for MOS1 (lower curve, red) and MOS2 (upper curve, blue) and residuals (bottom) when the line at 3.54 keV is *not added*. *Right*: Zoom at the range 3.0–4.0 keV.

However, significance of this results is not sufficient to confirm the hypothesis, they can be considered only as a successful sanity checks. More results are clearly needed to perform a convincing checking program described above.

A classical target for DM searches is the centre of our Galaxy. Its proximity allows to concentrate on the very central part and therefore, even for decaying DM, one can expect a significant gain in the signal if the DM distribution in the Milky Way happens to be steeper than a cored profile. The Galactic Center (GC) region has been extensively studied by the XMM and several mega-seconds of raw exposure exist. On the other hand, the GC region has strong X-ray emission, many complicated processes occur there [91–99]. In particular, the X-ray emitting gas may contain several thermal components with different temperatures; it may be more difficult to constraint reliably abundances of potassium and argon that in the case of intercluster medium. Therefore the GC data alone would hardly provide convincing detection of the DM signal, as even a relatively strong candidate line could be explained by astrophysical processes. In this paper we pose a different question: *Are the observations of the Galactic Center consistent with the dark matter interpretation of 3.53 keV line of [1, 2]?*

The DM interpretation of the 3.53 keV line in M31 and the Perseus cluster puts a *lower limit* on the flux from the GC. On the other hand, a non-detection of any signal in the off-center observations of the Milky Way halo (the blank sky dataset of [1]) provides an *upper limit* on the possible flux in the GC, given observational constraints on the DM distribution in the Galaxy. Therefore, even with all the uncertainties on the DM content of the involved objects, the expected signal from the GC is bounded from both sides and provides a non-trivial check for the DM interpretation of the 3.53 keV line.

We use XMM-Newton observations of the central 14' of the Galactic Center region (total clean exposure 1.4 Msec). We

find that the spectrum has a $\sim 5.7\sigma$ line-like excess at expected energy. The simultaneous fitting of GC, Perseus and M31 provides a $\sim 6.7\sigma$ significant signal at the same position, with the detected fluxes being consistent with the DM interpretation. The fluxes are also consistent with non-observation of the signal in the blank-sky and M31 off-center datasets, if one assumes steeper-than-cored DM profile (for example, NFW of Ref. [100]).

Below we summarize the details of our data analysis and discuss the results.

Data reduction. We use all archival data of the Galactic Center obtained by the EPIC MOS cameras [101] with Sgr A* less than 0.5' from the telescope axis (see Appendix, Table I). The data are reduced by standard SAS¹ pipeline, including screening for the time-variable soft proton flares by `espfilt`. We removed the observations taken during the MJD 54000–54500 due to strong flaring activity of Sgr A* in this period (see Fig. 3 in Appendix). The data reduction and preparation of the final spectra are similar to [1]. For each reduced observation we select a circle of radius 14' around Sgr A* and combine these spectra using the FTOOLS [102] procedure `addspec`.

Spectral modeling. To account for the cosmic-ray induced instrumental background we have subtracted the latest closed filter datasets (exposure: 1.30 Msec for MOS1 and 1.34 Msec for MOS2) [103]. The rescaling of the closed filter data has been performed to reduce to zero flux at energies $E > 10$ keV (see [104] for details). We model the resulting physical spectrum in the energy range 2.8–6.0 keV. The X-ray emission from the inner part of the Galactic Center contains both thermal and non-thermal components [93, 94]. Therefore, we chose to model the spectrum with the thermal plasma model

¹ v.13.5.0 <http://xmm.esa.int/sas>

(`vappec`), non-thermal powerlaw component modified by the `phabs` model to account the Galactic absorption.² We set abundances of all elements but Fe to zero and model known astrophysical lines with `gaussians` [1, 2, 106]. We selected the $\geq 2\sigma$ lines from the set of astrophysical lines of [2, 99]³. The intensities of the lines are allowed to vary, as are the central energies to account for uncertainties in detector gain and limited spectral resolution. We keep the same positions of the lines between two cameras.

The spectrum is binned to 45 eV to have about 4 bins per resolution element. The fit quality for the dataset is $\chi^2 = 108/100$ d.o.f. The resulting values for the main continuum components – the folded `powerlaw` index (for the integrated point source contribution), the temperature of the `vappec` model (~ 8 keV), and the absorption column density – agree well with previous studies [93, 94].

Results. The resulting spectra of the inner 14' of the Galactic Center shows a $\sim 5.7\sigma$ line-like excess at 3.539 ± 0.011 keV with the flux $(29 \pm 5) \times 10^{-6}$ cts/sec/cm² (see Fig. 1). It should be stressed that 1σ error-bars are obtained with the `xspec` command `error` (see the discussion below). The position of the excess is very close to similar excesses recently observed in the central part of the Andromeda galaxy (3.53 ± 0.03 keV) and the Perseus cluster (3.50 ± 0.04 keV), reported in [1], and is less than 2σ away from the one described in [2].

We also performed combined fits of the GC dataset with those of M31 and Perseus from [1]. As mentioned, the data reduction and modeling were performed very similarly, so we suffice with repeating that the inner part of M31 is covered by almost 1 Msec of cleaned MOS exposure, whereas a little over 500 ksec of clean MOS exposure was available for Perseus (see [1] for details).

We first perform a joint fit to the Galactic Center and M31, and subsequently to the Galactic Center, M31 and Perseus. In both cases, we start with the best-fit models of each individual analysis without any lines at 3.53 keV, and then add an additional gaussian to each model, allowing the energy to vary while keeping the same position between the models. The normalizations of this line for each dataset are allowed to vary independently. In this way, the addition of the line to the combination of Galactic Center, M31 and Perseus gives 4 extra degrees of freedom, which brings the joint significance to $\sim 6.7\sigma$.

To further investigate possible systematic error on the line parameters we took into account that the `gaussian` compo-

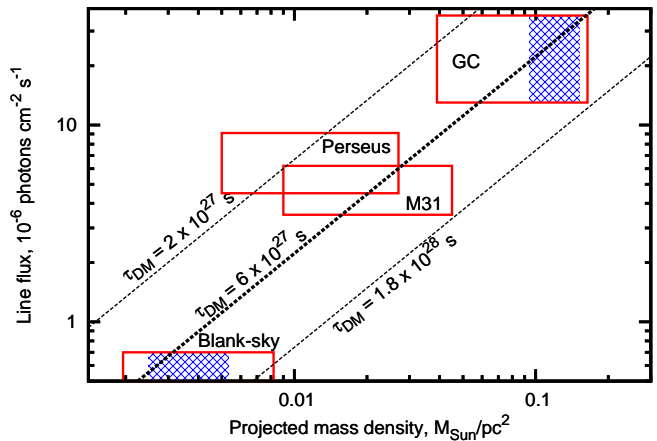


FIG. 2: The flux in 3.53 keV line in the spectra of GC (this work), Perseus cluster, M31 and the upper bound from blank sky (from [1]) as a function of the mass within the XMM’s field-of-view divided by the distance squared. The vertical sizes of the boxes are $\pm 1\sigma$ statistical error on the line’s flux. For GC this takes into account degeneracy with the width of the nearby Ar XVII complex; for the blank-sky dataset the 2σ upper bound on the flux is shown. The horizontal sizes of the boxes represent systematic error in mass modeling: projected mass density calculated using different literature models of DM distribution in the corresponding objects (Appendix A and refs. therein). Diagonal lines correspond to different lifetimes of DM particles, assuming decaying DM interpretation of the signal. Blue shaded regions give an example of the relation between the projected DM mass densities in the GC and in the blank-sky dataset based on the Milky Way mass model of Ref. [100] (its horizontal size indicates $\pm 0.5\sigma$ errors on the parameters of NFW distribution, derived in [100]). In particular, $\tau_{\text{DM}} \sim 6 \times 10^{27}$ sec is consistent with all datasets.

nent at 3.685 keV may describe not a single line, but a complex of lines (Table II). Using the `steppar` command we scanned over the two-dimensional grid of this `gaussian`’s intrinsic width and normalization of the line at 3.539 keV. We were able to find a new best fit with the 3.685 keV `gaussian` width being as large as 66 ± 15 eV. In this new minimum our line shifts to 3.50 ± 0.02 keV (as some of the photons were attributed to the 3.685 keV `gaussian`), has flux 24×10^{-6} cts/sec/cm² with 1σ confidence interval $(13 - 36) \times 10^{-6}$ cts/sec/cm². The significance of the line is $\Delta\chi^2 = 9.5$ (2.6σ for 2 d.o.f.). Although the width in the new minimum seems to be too large even for the whole complex of Ar XVII lines (see **Discussion**), we treat these change of line parameters as the estimates of systematic uncertainties. To reduce this systematics one has either to resolve or to reliably model a line complex around 3.685 keV instead of representing it as one wide `gaussian` component.

Discussion. The signal, found in the spectra of the central 14' of the GC is consistent with the DM interpretation of the spectral feature, reported in [1, 2] (Fig. 2). For example, given the mass modeling uncertainties in the individual objects the decaying DM with the lifetime $\tau_{\text{DM}} \sim 6 \times 10^{27}$ sec would

² The `Xspec` [105] v.12.8.0 is used for the spectral analysis.

³ Unlike [2] we do not include K XVIII lines at 3.47 and 3.51 keV to our model. See the discussion below

explain the signals from Perseus, M31 and non-observation of the line in the blank-sky dataset. Notice that in the clusters outskirts the hydrostatic mass may be under-estimated (see e.g. (see e.g. [107])). This would only improve the consistency between various data sets.

The ratio of the flux of the GC signal and the upper bound in the blank-sky observation is consistent for steeper-than-cored DM density profiles of the Milky Way (Table III). For example, the central value of the flux in the GC would correspond to the expectation from the Milky Way mass modelling of Ref. [100]. The predictions of all NFW and Einasto profiles in Table III are within 1σ range for the GC flux if one assumes blank-sky flux at the upper bound (0.7×10^{-6} cts/sec/cm²).

As mentioned in the **Results**, there is a degeneracy between the width of Ar XVII complex around 3.685 keV and the normalization of the line in question. If we allow the width of the Ar XVII line to vary freely we can decrease significance of the line at 3.539 keV to about 2σ . However, in this case the width of the gaussian at 3.685 keV should be 95 – 130 eV, which is significantly larger than we obtain when simulating complex of four Ar XVII lines via `fakeit` command. In addition, in this case the total flux of the line at 3.685 keV becomes *higher* than the fluxes in the lines at 3.130 and 3.895 in contradiction with the atomic data (Table II).

Another way to decrease the significance of the line at 3.539 is to assume the presence of potassium (K XVIII) ion with a line at 3.515 keV and a smaller line at 3.47 keV. If one considers the abundance of potassium as a completely free parameter (as it was done in [106] for the Chandra data of the Galactic Center), one can find an acceptable fit of the XMM GC data without an additional line at 3.539 keV.

One may attempt to predict the ratio of fluxes of the K XVIII line and of the strong lines in the interval 3–4 keV (i.e. Ar XVII, Ca XIX, Ca XX, S XVI, etc.) using known ratio of emissivities and assuming certain (solar?) ratio of abundances (similarly to the analysis of the Section 4 of [2]). The problem with such an approach is that neither in the case of the GC, nor in the case of galaxy clusters the emission is described well by a single-temperature model. In [2] a multi-temperature fit to the continuum is found. Based on this model, the authors of [2] conclude that strongly super-solar abundance of K XVIII is required to explain the observed excess.

We did not find a good multi-temperature model of the GC emission that would explain the observed ratio of fluxes of the strong lines. Using flux in one of the strong lines, assuming certain temperature of the plasma and solar ratio of abundances of the element one can predict the flux K XVIII lines. However, for different temperatures and for different strong

lines this procedure predictions vary by more than an order of magnitude. Therefore, it is not possible to define reliably the abundance of potassium in the GC and to attribute the flux in the line 3.539 keV to K XVIII ion or to some other unidentified source (dark matter?). Therefore, based on the GC data

alone we cannot either claim the existence of an unidentified spectral line no top of the element lines, nor constrain it.

However, if we are to explain the presence of this line in the spectra by the presence of K XVIII, we have to build a model that consistently explains the fluxes in this line in different astronomical environments: in galaxy clusters (in particular Perseus) at all off-center distances, from central regions [2] to cluster outskirts up to the virial radius [1]; GC; and the central part of M31. On the other hand, this transition *should not* be excited in the outskirts of the Milky Way and of M31. For such a model it is not enough to find the values of temperatures and abundances that would explain the observed flux in each object individually. In particular, in the case of M31 there are no strong astrophysical lines between 3 and 4 keV. However, the powerlaw continuum is well determined by fitting the data over a wider range of energies (from 2 to 8 keV) and allows to clearly detect the presence of the line at 3.53 ± 0.03 keV with $\Delta\chi^2 = 13$ [1].

We conclude that although it is hard to exclude completely astrophysical origin of 3.539 keV line in the spectrum of the GC, the DM interpretation of the signal observed in Perseus and M31 [1] and in the stacked spectra of galaxy clusters [2] is fully consistent with the GC data. Moreover, GC data rather supports this interpretation as the line is not only observed there at the same energy, but also its flux is consistent with the expectations about the DM content of the GC for the whole class of the Milky Way mass models.

To check further this intriguing possibility, a more precise resolution of the atomic lines (e.g. with the forth-coming *Astro-H* mission [108]), an independent measurements of the relative abundance of elements in the GC region, or analysis of additional deep exposure dataset of DM-dominated objects is needed.

Acknowledgments. The work of D. I. was supported by part by the Swiss National Science Foundation grant SCOPE IZ7370-152581, the Program of Cosmic Research of the National Academy of Sciences of Ukraine, the State Programme of Implementation of Grid Technology in Ukraine and the grant of President of Ukraine for young scientists. The work of J. F. was supported by the De Sitter program at Leiden University with funds from NWO. This research is part of the “Fundamentals of Science” program at Leiden University.

[1] A. Boyarsky, O. Ruchayskiy, D. Iakubovskiy, and J. Franse, ArXiv e-prints (2014).

[2] E. Bulbul, M. Markevitch, A. Foster, R. K. Smith, M. Loewen-

- stein, et al., 1402.2301 (2014).
- [3] H. Ishida, K. S. Jeong, and F. Takahashi, *Physics Letters B* **732**, 196 (2014).
 - [4] D. P. Finkbeiner and N. Weiner, ArXiv e-prints (2014).
 - [5] T. Higaki, K. S. Jeong, and F. Takahashi, *Physics Letters B* **733**, 25 (2014).
 - [6] J. Jaeckel, J. Redondo, and A. Ringwald, *Phys. Rev. D* **89**, 103511 (2014).
 - [7] M. Czerny, T. Higaki, and F. Takahashi, *Journal of High Energy Physics* **5**, 144 (2014).
 - [8] H. M. Lee, S. C. Park, and W.-I. Park, ArXiv e-prints (2014).
 - [9] K. N. Abazajian, *Physical Review Letters* **112**, 161303 (2014).
 - [10] R. Krall, M. Reece, and T. Roxlo, ArXiv e-prints (2014).
 - [11] C. El Aisati, T. Hambye, and T. Scarna, ArXiv e-prints (2014).
 - [12] K. Hamaguchi, M. Ibe, T. T. Yanagida, and N. Yokozaki, ArXiv e-prints (2014).
 - [13] K. Kong, J.-C. Park, and S. C. Park, ArXiv e-prints (2014).
 - [14] M. T. Frandsen, F. Sannino, I. M. Shoemaker, and O. Svendsen, *JCAP* **5**, 033 (2014).
 - [15] S. Baek and H. Okada, ArXiv e-prints (2014).
 - [16] K. Nakayama, F. Takahashi, and T. T. Yanagida, ArXiv e-prints (2014).
 - [17] K.-Y. Choi and O. Seto, ArXiv e-prints (2014).
 - [18] M. Cicoli, J. P. Conlon, M. C. D. Marsh, and M. Rummel, ArXiv e-prints (2014).
 - [19] B. Shuve and I. Yavin, *Phys. Rev. D* **89**, 113004 (2014).
 - [20] C. Kolda and J. Unwin, ArXiv e-prints (2014).
 - [21] R. Allahverdi, B. Dutta, and Y. Gao, ArXiv e-prints (2014).
 - [22] A. G. Dias, A. C. B. Machado, C. C. Nishi, A. Ringwald, and P. Vaudrevange, *Journal of High Energy Physics* **6**, 37 (2014).
 - [23] N.-E. Bomark and L. Roszkowski, ArXiv e-prints (2014).
 - [24] S. Pei Liew, *JCAP* **5**, 044 (2014).
 - [25] K. Nakayama, F. Takahashi, and T. T. Yanagida, *Physics Letters B* **734**, 178 (2014).
 - [26] Z. Kang, P. Ko, T. Li, and Y. Liu, ArXiv e-prints (2014).
 - [27] H. Okada, ArXiv e-prints (2014).
 - [28] S. V. Demidov and D. S. Gorbunov, ArXiv e-prints (2014).
 - [29] F. S. Queiroz and K. Sinha, *Physics Letters B* **735**, 69 (2014).
 - [30] E. Dudas, L. Heurtier, and Y. Mambrini, ArXiv e-prints (2014).
 - [31] K. S. Babu and R. N. Mohapatra, *Phys. Rev. D* **89**, 115011 (2014).
 - [32] K. Prasad Modak, ArXiv e-prints (2014).
 - [33] J. M. Cline, Y. Farzan, Z. Liu, G. D. Moore, and W. Xue, ArXiv e-prints (2014).
 - [34] H. Okada and T. Toma, ArXiv e-prints (2014).
 - [35] J. L. Rosner, ArXiv e-prints (2014).
 - [36] H. M. Lee, ArXiv e-prints (2014).
 - [37] J. Barry, J. Heeck, and W. Rodejohann, ArXiv e-prints (2014).
 - [38] D. J. Robinson and Y. Tsai, ArXiv e-prints (2014).
 - [39] J. P. Conlon and F. V. Day, ArXiv e-prints (2014).
 - [40] J. Kubo, K. Sham Lim, and M. Lindner, ArXiv e-prints (2014).
 - [41] M. Drewes, ArXiv e-prints (2014).
 - [42] S. Baek, P. Ko, and W.-I. Park, ArXiv e-prints (2014).
 - [43] K. Nakayama, F. Takahashi, and T. T. Yanagida, ArXiv e-prints (2014).
 - [44] J. Bateman, I. McHardy, A. Merle, T. R. Morris, and H. Ulbricht, ArXiv e-prints (2014).
 - [45] S. Chakraborty, D. K. Ghosh, and S. Roy, ArXiv e-prints (2014).
 - [46] M. Lattanzi, R. A. Lineros, and M. Taoso, ArXiv e-prints (2014).
 - [47] M. Kawasaki, N. Kitajima, and F. Takahashi, ArXiv e-prints (2014).
 - [48] N. Chen, Z. Liu, and P. Nath, ArXiv e-prints (2014).
 - [49] J. P. Conlon and A. J. Powell, ArXiv e-prints (2014).
 - [50] H. Ishida and H. Okada, ArXiv e-prints (2014).
 - [51] C.-Q. Geng, D. Huang, and L.-H. Tsai, ArXiv e-prints (2014).
 - [52] A. Abada, G. Arcadi, and M. Lucente, ArXiv e-prints (2014).
 - [53] A. Abada, V. De Romeri, and A. M. Teixeira, ArXiv e-prints (2014).
 - [54] H. Baer, K.-Y. Choi, J. E. Kim, and L. Roszkowski, ArXiv e-prints (2014).
 - [55] C.-W. Chiang and T. Yamada, ArXiv e-prints (2014).
 - [56] A. Ringwald, ArXiv e-prints (2014).
 - [57] B. Dutta, I. Gogoladze, R. Khalid, and Q. Shafi, ArXiv e-prints (2014).
 - [58] A. Boyarsky, O. Ruchayskiy, M. G. Walker, S. Riemer-Sørensen, and S. H. Hansen, *MNRAS* **407**, 1188 (2010).
 - [59] A. Boyarsky, A. Neronov, O. Ruchayskiy, and I. Tkachev, *Phys. Rev. Lett.* **104**, 191301 (2010).
 - [60] A. Boyarsky, O. Ruchayskiy, D. Iakubovskiy, A. V. Maccio', and D. Malyshev, 0911.1774 (2009).
 - [61] A. Boyarsky, A. Neronov, O. Ruchayskiy, M. Shaposhnikov, and I. Tkachev, *Phys. Rev. Lett.* **97**, 261302 (2006).
 - [62] A. Boyarsky, J. W. den Herder, O. Ruchayskiy, et al., 0906.1788 (2009), a white paper submitted in response to the Fundamental Physics Roadmap Advisory Team (FPR-AT) Call for White Papers.
 - [63] K. N. Abazajian, 0903.2040 (2009), white paper submitted to the Astro 2010 Decadal Survey, Cosmology and Fundamental Physics Science.
 - [64] A. Boyarsky, D. Iakubovskiy, and O. Ruchayskiy, *Phys. Dark Univ.* **1**, 136 (2012).
 - [65] K. Abazajian, G. M. Fuller, and W. H. Tucker, *Astrophys. J.* **562**, 593 (2001).
 - [66] A. D. Dolgov and S. H. Hansen, *Astropart. Phys.* **16**, 339 (2002).
 - [67] A. Boyarsky, A. Neronov, O. Ruchayskiy, and M. Shaposhnikov, *MNRAS* **370**, 213 (2006).
 - [68] A. Boyarsky, A. Neronov, O. Ruchayskiy, and M. Shaposhnikov, *Phys. Rev. D* **74**, 103506 (2006).
 - [69] S. Riemer-Sørensen, S. H. Hansen, and K. Pedersen, *ApJ* **644**, L33 (2006).
 - [70] C. R. Watson, J. F. Beacom, H. Yuksel, and T. P. Walker, *Phys. Rev. D* **74**, 033009 (2006).
 - [71] S. Riemer-Sørensen, K. Pedersen, S. H. Hansen, and H. Dahle, *Phys. Rev. D* **76**, 043524 (2007).
 - [72] A. Boyarsky, J. Nevalainen, and O. Ruchayskiy, *A&A* **471**, 51 (2007).
 - [73] K. Abazajian and S. M. Koushiappas, *Phys. Rev. D* **74**, 023527 (2006).
 - [74] A. Boyarsky, O. Ruchayskiy, and M. Markevitch, *ApJ* **673**, 752 (2008).
 - [75] A. Boyarsky, J. W. den Herder, A. Neronov, and O. Ruchayskiy, *Astropart. Phys.* **28**, 303 (2007).
 - [76] H. Yuksel, J. F. Beacom, and C. R. Watson, *Phys. Rev. Lett.* **101**, 121301 (2008).
 - [77] A. Boyarsky, D. Iakubovskiy, O. Ruchayskiy, and V. Savchenko, *MNRAS* **387**, 1361 (2008).
 - [78] A. Boyarsky, D. Malyshev, A. Neronov, and O. Ruchayskiy, *MNRAS* **387**, 1345 (2008).
 - [79] M. Loewenstein, A. Kusenko, and P. L. Biermann, *ApJ* **700**, 426 (2009).
 - [80] S. Riemer-Sørensen and S. H. Hansen, *A&A* **500**, L37 (2009).
 - [81] M. Loewenstein and A. Kusenko, *Astrophys. J.* **714**, 652 (2010).

- [82] A. Boyarsky, O. Ruchayskiy, D. Iakubovskiy, M. G. Walker, S. Riemer-Sørensen, and S. H. Hansen, *MNRAS* **407**, 1188 (2010).
- [83] N. Mirabal and D. Nieto, ArXiv e-prints (2010).
- [84] N. Mirabal, *MNRAS* **409**, L128 (2010).
- [85] D. A. Prokhorov and J. Silk, 1001.0215 (2010).
- [86] E. Borriello, M. Paolillo, G. Miele, G. Longo, and R. Owen, *Mon.Not.Roy.Astron.Soc.* **425**, 1628 (2012).
- [87] C. R. Watson, Z. Li, and N. K. Polley, *JCAP* **3**, 18 (2012).
- [88] M. Loewenstein and A. Kusenko, *Astrophys.J.* **751**, 82 (2012).
- [89] A. Kusenko, M. Loewenstein, and T. T. Yanagida, ArXiv e-prints (2012).
- [90] S. Horiuchi, P. J. Humphrey, J. Onorbe, K. N. Abazajian, M. Kaplinghat, et al., *Phys.Rev.* **D89**, 025017 (2013).
- [91] K. Koyama, H. Awaki, H. Kunieda, S. Takano, and Y. Tawara, *Nature* **339**, 603 (1989).
- [92] K. Koyama, Y. Maeda, T. Sonobe, T. Takeshima, Y. Tanaka, and S. Yamauchi, *PASJ* **48**, 249 (1996).
- [93] H. Kaneda, K. Makishima, S. Yamauchi, K. Koyama, K. Matsuzaki, and N. Y. Yamasaki, *ApJ* **491**, 638 (1997).
- [94] M. P. Muno, J. S. Arabadjis, F. K. Baganoff, M. W. Bautz, W. N. Brandt, P. S. Broos, E. D. Feigelson, G. P. Garmire, M. R. Morris, and G. R. Ricker, *ApJ* **613**, 1179 (2004).
- [95] K. Koyama, Y. Hyodo, T. Inui, H. Nakajima, H. Matsumoto, T. G. Tsuru, T. Takahashi, Y. Maeda, N. Y. Yamazaki, H. Murakami, et al., *PASJ* **59**, 245 (2007).
- [96] M. P. Muno, F. K. Baganoff, W. N. Brandt, S. Park, and M. R. Morris, *ApJ* **656**, L69 (2007).
- [97] M. Revnivtsev, S. Sazonov, E. Churazov, W. Forman, A. Vikhlinin, and R. Sunyaev, *Nature* **458**, 1142 (2009).
- [98] G. Ponti, R. Terrier, A. Goldwurm, G. Belanger, and G. Trap, *ApJ* **714**, 732 (2010).
- [99] H. Uchiyama, M. Nobukawa, T. G. Tsuru, and K. Koyama, *PASJ* **65**, 19 (2013).
- [100] M. Weber and W. de Boer, *A&A* **509**, A25 (2010).
- [101] M. J. L. Turner, A. Abbey, M. Arnaud, M. Balasini, M. Barbera, E. Belsole, P. J. Bennie, J. P. Bernard, G. F. Bignami, M. Boer, et al., *A&A* **365**, L27 (2001).
- [102] Irby, B., The ftools webpage, HeaSoft, http://heasarc.gsfc.nasa.gov/docs/software/ftools/ftools_menu.html (2008).
- [103] *Repository of xmm-newton epic filter wheel closed data*, http://xmm2.esac.esa.int/external/xmm_sw_cal/background/filter_closed/index.shtml.
- [104] J. Nevalainen, M. Markevitch, and D. Lumb, *ApJ* **629**, 172 (2005).
- [105] K. A. Arnaud, in *Astronomical Data Analysis Software and Systems V*, edited by G. H. Jacoby and J. Barnes (San Francisco, ASP, 1996), vol. 101 of *A.S.P. Conference Serie*, p. 17.
- [106] S. Riemer-Sørensen, ArXiv e-prints (2014).
- [107] N. Okabe, K. Umetsu, T. Tamura, Y. Fujita, M. Takizawa, Y.-Y. Zhang, K. Matsushita, T. Hamana, Y. Fukazawa, T. Futamase, et al., ArXiv e-prints (2014).
- [108] T. Takahashi, K. Mitsuda, R. Kelley, H. Aharonian, F. Aarts, et al., 1210.4378 (2012).
- [109] T. Abbey, J. Carpenter, A. Read, A. Wells, Xmm Science Centre, and Swift Mission Operations Center, in *The X-ray Universe 2005*, edited by A. Wilson (2006), vol. 604 of *ESA Special Publication*, p. 943.
- [110] *Xmm-newton epic mos1 ccd6 update*, http://xmm.esac.esa.int/external/xmm_news/items/MOS1-CCD6/.
- [111] D. Porquet, N. Grosso, P. Predehl, G. Hasinger, F. Yusef-Zadeh, B. Aschenbach, G. Trap, F. Melia, R. S. Warwick, A. Goldwurm, et al., *A&A* **488**, 549 (2008).
- [112] J. F. Navarro, C. S. Frenk, and S. D. M. White, *Astrophys. J.* **462**, 563 (1996).
- [113] J. F. Navarro, C. S. Frenk, and S. D. M. White, *ApJ* **490**, 493 (1997).
- [114] J. Einasto, *Trudy Astrofizicheskogo Instituta Alma-Ata* **5**, 87 (1965).
- [115] J. F. Navarro, E. Hayashi, C. Power, A. R. Jenkins, C. S. Frenk, S. D. M. White, V. Springel, J. Stadel, and T. R. Quinn, *MNRAS* **349**, 1039 (2004).
- [116] A. D. Ludlow, J. F. Navarro, M. Boylan-Kolchin, P. E. Bett, R. E. Angulo, M. Li, S. D. M. White, C. Frenk, and V. Springel, *MNRAS* **432**, 1103 (2013).
- [117] A. A. Dutton and A. V. Macciò, *MNRAS* **441**, 3359 (2014).
- [118] A. Burkert, *ApJ* **447**, L25+ (1995).
- [119] G. Gentile, P. Salucci, U. Klein, D. Vergani, and P. Kalberla, *MNRAS* **351**, 903 (2004).
- [120] S. M. Kent, *AJ* **91**, 1301 (1986).
- [121] M. R. Merrifield, *AJ* **103**, 1552 (1992).
- [122] C. Alcock, R. A. Allsman, T. S. Axelrod, D. P. Bennett, K. H. Cook, K. C. Freeman, K. Griest, J. A. Guern, M. J. Lehner, S. L. Marshall, et al., *ApJ* **461**, 84 (1996).
- [123] G. Battaglia, A. Helmi, H. Morrison, P. Harding, E. W. Olszewski, M. Mateo, K. C. Freeman, J. Norris, and S. A. Shectman, *MNRAS* **370**, 1055 (2006).
- [124] M. C. Smith et al., *Mon. Not. Roy. Astron. Soc.* **379**, 755 (2007).
- [125] X. X. Xue et al. (SDSS), *Astrophys. J.* **684**, 1143 (2008).
- [126] Y. Sofue, M. Honma, and T. Omodaka, *PASJ* **61**, 227 (2009).
- [127] P. J. McMillan, *MNRAS* **414**, 2446 (2011).
- [128] N. Bernal and S. Palomares-Ruiz, *JCAP* **1**, 006 (2012).
- [129] A. J. Deason, V. Belokurov, N. W. Evans, and J. An, *MNRAS* **424**, L44 (2012).
- [130] F. Nesti and P. Salucci, *JCAP* **7**, 016 (2013).

	ObsID	Off-center angle arcmin	Cleaned exposure MOS1/MOS2 [ksec]	FoV [arcmin ²] MOS1/MOS2
1	0111350101	0.017	40.8/40.7	570.5/570.3
2	0111350301	0.017	7.2/6.8	565.8/573.4
3	0112972101	0.087	20.8/21.4	571.4/572.0
4	0202670501	0.003	21.4/26.5	564.9/573.4
5	0202670601	0.003	29.6/31.1	563.8/574.1
6	0202670701	0.003	76.0/80.0	570.4/573.3
7	0202670801	0.003	86.9/91.0	569.2/572.8
8	0402430301 ^a	0.002	57.6/60.2	475.8/572.1
9	0402430401 ^a	0.002	37.3/37.8	476.2/572.3
10	0402430701 ^a	0.002	23.1/25.2	478.5/573.1
11	0504940201 ^a	0.286	7.7/8.5	487.6/572.6
12	0505670101 ^a	0.002	65.7/73.7	472.0/573.2
13	0554750401	0.003	31.6/31.5	483.4/574.0
14	0554750501	0.003	39.6/39.2	487.0/574.0
15	0554750601	0.003	35.5/36.4	487.0/573.3
16	0604300601	0.003	28.9/30.0	487.1/573.1
17	0604300701	0.003	35.1/37.1	487.4/572.7
18	0604300801	0.003	34.9/34.2	487.8/572.5
19	0604300901	0.003	21.1/20.7	485.1/574.0
20	0604301001	0.003	35.3/38.6	487.4/573.6
21	0658600101	0.078	46.5/47.6	477.2/573.0
22	0658600201	0.078	38.3/39.7	478.3/572.3
23	0674600601	0.002	9.0/9.4	483.2/573.8
24	0674600701	0.003	12.8/13.5	484.9/575.0
25	0674600801	0.003	17.9/18.2	481.4/574.1
26	0674601001	0.003	20.0/21.5	480.9/573.7
27	0674601101	0.003	10.1/10.7	480.4/573.8

TABLE I: Properties of the XMM observations of the Galactic Center used in our analysis. We have only used observations with centers located within 0.5' around Sgr A*. The difference in FoVs between MOS1 and MOS2 cameras is due to the loss CCD6 in MOS1 camera, see [109, 110] for details.

^a Observation discarded from our analysis due to flares in Sgr a*, see Fig. 3 and [111].

Supplementary material

Appendix A: Profiles of Milky Way galaxy

The distribution of dark matter in galaxies, galaxy groups and galaxy clusters can be described by several density profiles. In this work we concentrated on four popular choices for dark matter density profiles.

I. Numerical (N-body) simulations of the cold dark matter model have shown that the dark matter distribution in all relaxed halos can be fitted with the universal Navarro-Frenk-White (NFW) profile [112, 113]:

$$\rho_{\text{NFW}}(r) = \frac{\rho_s r_s}{r(1 + r/r_s)^2} \quad (\text{A1})$$

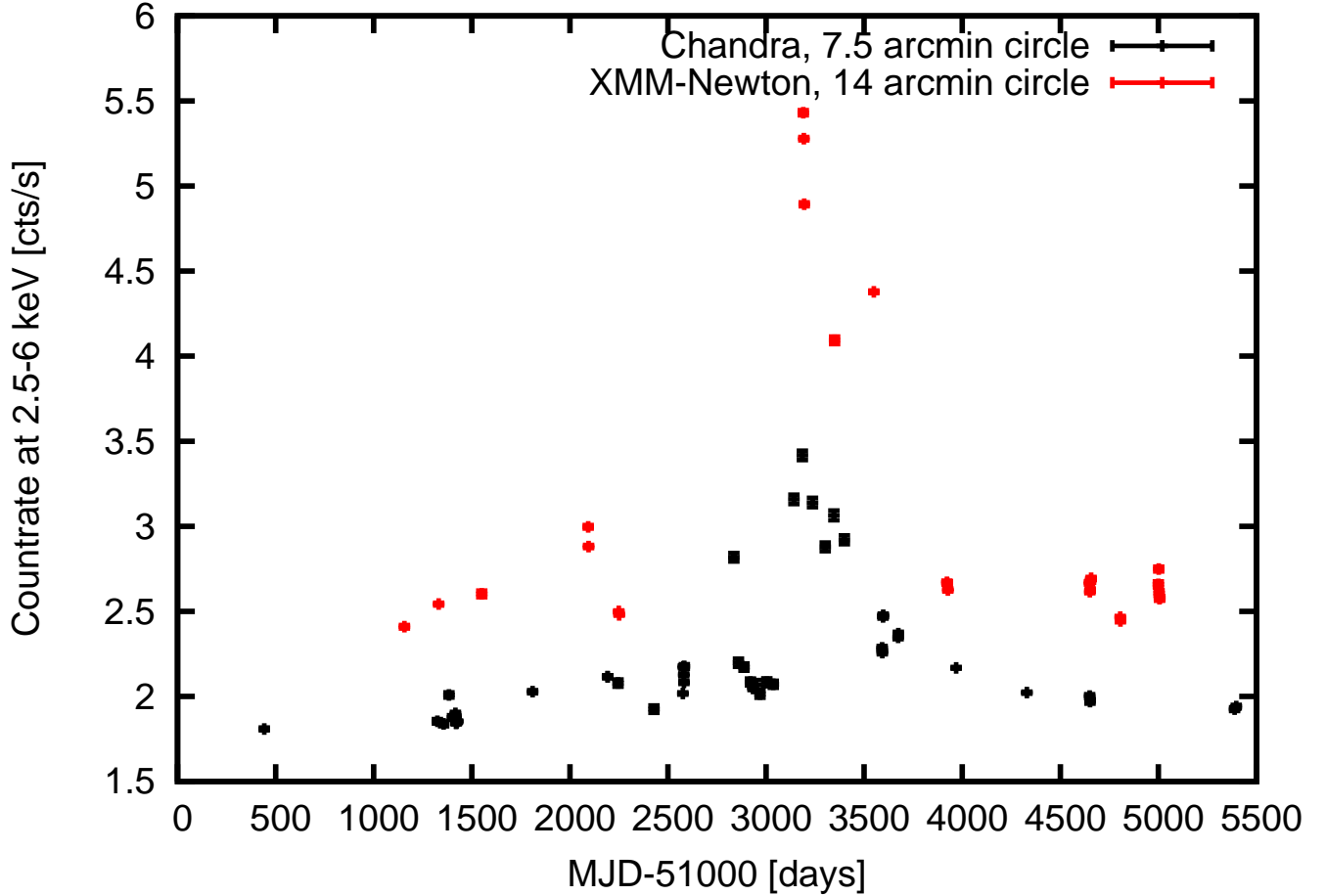


FIG. 3: Average count rates on regions centered in Sgr a* using *XMM-Newton* (red) and *Chandra* (black). The enhancement at MJD 54000-54500 are due to strong flaring activity of Sgr a*, see [111] for details. 5 *XMM-Newton* observations during this flaring period were discarded from our analysis, see Table I for details.

parametrised by ρ_s and r_s .

II. A generalization of NFW profile (EIN) proposed by J. Einasto [114] consistent with recent high-resolution N-body simulations [115–117]:

$$\rho_{\text{EIN}}(r) = \rho_{\odot} \exp\left(-\frac{2}{\alpha} \left[\left(\frac{r}{r_{\text{Ein}}}\right)^{\alpha} - \left(\frac{r_{\odot}}{r_{\text{Ein}}}\right)^{\alpha}\right]\right). \quad (\text{A2})$$

III. The Burkert (BURK) profile [118] has been shown to be successful in explaining the kinematics of disk systems (e.g. [119]):

$$\rho_{\text{BURK}}(r) = \frac{\rho_B r_B^3}{(r_B + r)(r_B^2 + r^2)}. \quad (\text{A3})$$

IV. Another common parametrizations of cored profiles are given by the pseudo-isothermal (ISO) profile [120]

$$\rho_{\text{ISO}}(r) = \frac{\rho_c}{1 + r^2/r_c^2}. \quad (\text{A4})$$

Ion	Position keV	Upper level	Lover level	Emissivity ph cm ³ s ⁻¹	T _e peak keV	Relative intensity
Ca XIX	3.902	7	1	3.913e-18	2.725e+0	0.59
Ca XIX	3.883	5	1	6.730e-19	2.725e+0	0.10
Ca XIX	3.861	2	1	1.242e-18	2.165e+0	0.19
Ar XVII	3.685	13	1	8.894e-19	1.719e+0	0.13
Ar XVII	3.683	11	1	3.729e-20	1.719e+0	0.01
Ar XVII	3.618	10077	2	3.627e-20	1.366e+0	0.01
Ar XVII	3.617	10078	3	9.355e-20	1.366e+0	0.01
Ar XVIII	3.323	4	1	4.052e-18	3.431e+0	0.61
Ar XVIII	3.318	3	1	2.061e-18	3.431e+0	0.31
S XVI	3.276	12	1	9.146e-19	2.165e+0	0.14
Ar XVII	3.140	7	1	6.604e-18	1.719e+0	1.00
Ar XVII	3.126	6	1	7.344e-19	1.719e+0	0.11
Ar XVII	3.124	5	1	1.018e-18	1.719e+0	0.15
S XVI	3.107	7	1	3.126e-18	2.165e+0	0.47
S XVI	3.106	6	1	1.584e-18	2.165e+0	0.24
Ar XVII	3.104	2	1	2.575e-18	1.719e+0	0.39
S XV	3.101	37	1	7.252e-19	1.366e+0	0.11
S XV	3.033	23	1	1.556e-18	1.366e+0	0.24

TABLE II: List of astrophysical lines at 3-4 keV expected in our model. Basic line parameters such as energy, type of ion, type of transition – are taken from AtomDB database. Only the strongest lines are shown. Close lines of the same ion are grouped with horizontal lines.

Because we reside in the inner part of Milky Way dark matter halo, it is the only object whose dark matter decay signal would be spread across the whole sky. The dark matter column density for the Milky Way halo is calculated using the expression [72]

$$\mathcal{S}_{\text{DM}}^{MW}(\phi) = \int_0^{\infty} \rho_{\text{DM}} \left(\sqrt{r_{\odot}^2 + z^2 - 2zr_{\odot} \cos \phi} \right) dz \quad (\text{A5})$$

where ϕ is the off-the-Galactic-center region, so that for the direction with galactic coordinates (l, b)

$$\cos \phi = \cos b \cos l. \quad (\text{A6})$$

and $r_{\odot} = 8$ kpc is the distance from the Earth to the Sun.

It can be seen (e.g. [61, 72, 78]) that the function $\mathcal{S}_{\text{DM}}^{MW}$ can change only by a factor of few, when moving from the Galactic center ($\phi = 0^\circ$) to the anti-center ($\phi = 180^\circ$). That is, the Milky Way contribution to the decay is an all-sky signal.

The mass modeling of the Milky Way is continuously updated and improved (see e.g. [100, 121–130]). In Table III we summarize recent results. For each of the profiles the dark matter column density is calculated using the expression (A5). The results are shown in Fig. 4. The behaviour of cored (ISO, Burkert) and cusped (NFW, Einasto) profiles differs at small ϕ .

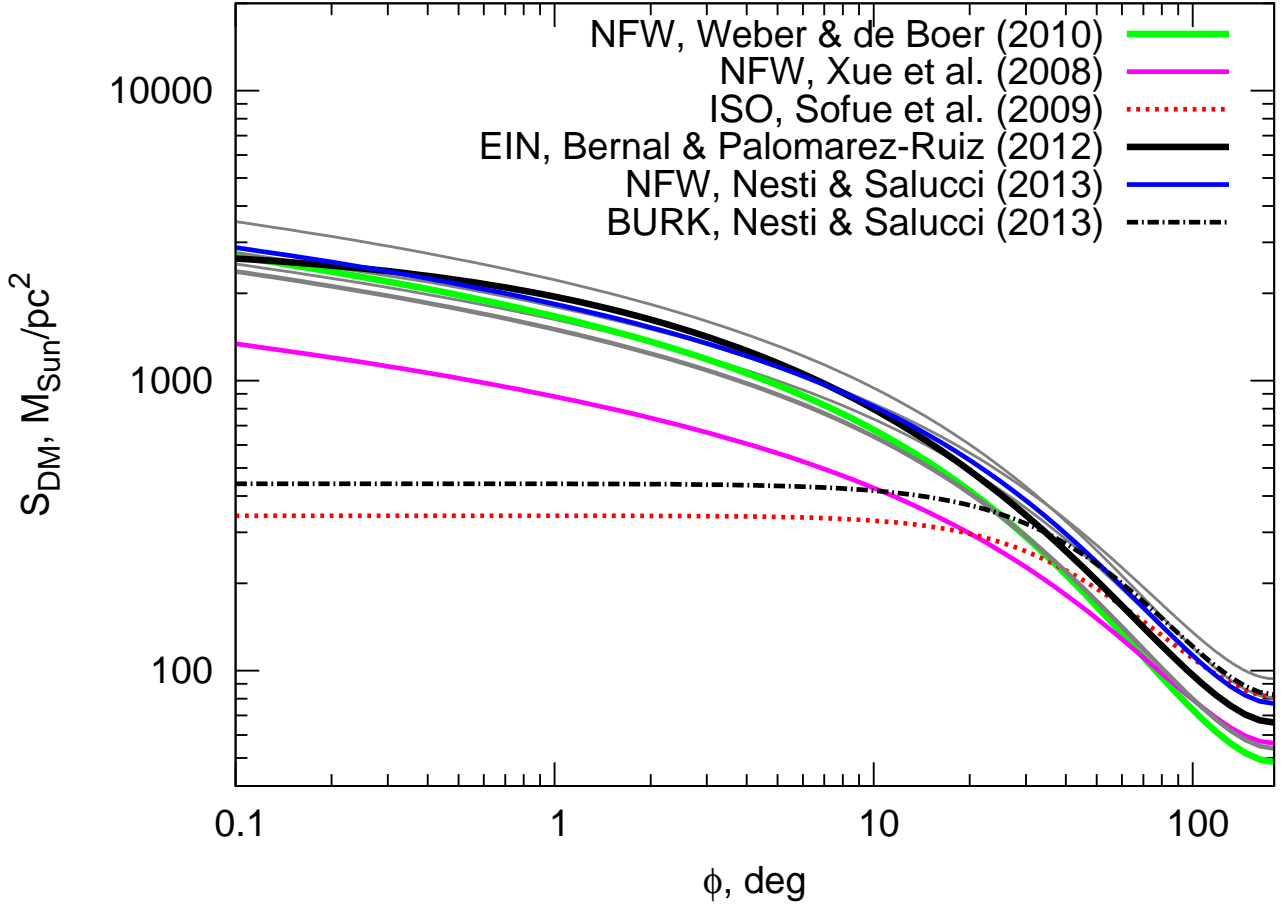


FIG. 4: Known dark matter distributions for Milky Way galaxy.

Reference	Type	ρ_* , $10^6 M_\odot / \text{kpc}^3$	r_* , kpc	r_\odot , kpc	S_{GC} M_\odot / pc^2	S_{BS} M_\odot / pc^2	S_{GC}/S_{BS} ratio
[124]	NFW	27.2 ± 15.0	10.2 ± 6.1	8.5	3402^{+2376}_{-755}	102^{+105}_{-66}	33.4 (27.9-73.5)
[129]	NFW	28.0	10.4	8.5	3579	109	32.8
[100]	NFW	20.4 ± 2.6	10.8 ± 3.4	8.33 ± 0.35	2727^{+691}_{-726}	87^{+36}_{-30}	31.3 (27.7-35.1)
[128]	EIN	10.4	20	8.3	2574	95	27.1
[123]	NFW	13.3	14.7 ± 0.7	8.0	2501^{+126}_{-127}	101^{+7}_{-8}	24.8 (24.3-25.5)
[127]	NFW	12.5 ± 6.0	17.0 ± 3.9	8.33 ± 0.35	2721^{+1057}_{-904}	112^{+53}_{-42}	24.2 (22.9-26.0)
[130]	NFW	$14.0^{+29}_{-9.3}$	$16.1^{+17.0}_{-7.8}$	8.08 ± 0.2	2893^{+6040}_{-1460}	120^{+302}_{-69}	24.1 (21.2-28.1)
[125] ^a	NFW	4.74 ± 0.57	21.0 ± 3.2	8.0	1282^{+165}_{-167}	59 ± 9	21.7 (21.3-22.3)
[130]	BURK	41.3^{+62}_{-16}	$9.26^{+2.9}_{-0.93}$	$7.94^{+0.36}_{-0.24}$	481^{+429}_{-104}	144^{+173}_{-39}	3.3 (2.9-3.6)
[126]	ISO	24.5 ± 2.5	5.5 ± 0.6	8.0	326^{+30}_{-28}	104 ± 14	3.1 (3.0-3.3)

TABLE III: Parameters of dark matter profiles for Milky Way galaxy. Here, ρ_* and r_* denote the characteristic density and radius of dark matter distributions (ρ_s and r_s for NFW; core radius and central density for the Burkert profile, etc. For the Einasto profile [128] the inner slope $\alpha = 0.17$ is used). r_\odot is the solar distance to the Galactic Centre. S_{GC} and S_{BS} are the FoV and exposure averaged column densities from our current dataset (GC) and blank-sky dataset of [1] (BS), respectively. Wherever 1σ errors on the derived parameters ρ_* and r_* are given in the original references, we vary these parameters within $\pm 0.5\sigma$ (to account for the degeneracy between parameters) and show in parentheses the range of variation of S and GC to BS ratio.

^a Mass-concentration relation between distribution parameters is assumed.